Separation and Purification Technology 299 (2022) 121789

Contents lists available at ScienceDirect

Separation and Purification Technology

journal homepage: www.elsevier.com/locate/seppur

Layered potassium calcium phosphate with multiple exchangeable cations for Sr(II) and Co(II) removal from water

Zeqiu Li [a], Eleazer L. Vivas [a], Chenyang Yang [a], Yong Jae Suh [b,c,*], Kuk Cho [a,*]

[a] Department of Environmental Engineering, Pusan National University, 2 Busandaehak-ro, 63beon-gil, Geumjeong-gu, Busan 46241, Republic of Korea
[b] Resources Utilization Division, Korea Institute of Geoscience and Mineral Resources, 124 Gwahak-ro, Yuseong-gu, Daejeon 34132, Republic of Korea
[c] Department of Resources Engineering, Korea University of Science and Technology, 217 Gajeong-ro, Yuseong-gu, Daejeon 34113, Republic of Korea

ARTICLE INFO

Keywords:
Cobalt
Strontium
Radionuclide
Glaserite
Structural transformation
Separation

ABSTRACT

Developing adsorbents with fast uptake rates and high adsorption capacities for both Sr^{2+} and Co^{2+} is a major challenge for treating radioactive wastewater. Traditional calcium phosphates (CaPs) can adsorb Sr^{2+} and Co^{2+} but their adsorption performance is limited by their compact structures. Because of the looser structure and the presence of more exchangeable cations than other CaPs, layered potassium calcium phosphate ($K_3HCa(PO_4)_2$, KCaP) would be appropriate for removing Sr^{2+} and Co^{2+} from wastewater. KCaP demonstrated fast uptake (94.1 % Sr^{2+} in 120 min and 96.6 % Co^{2+} in 10 min) and remarkable adsorption capacity (384 mg g^{-1} for Sr^{2+} and 382 mg g^{-1} for Co^{2+}). It also exhibited high distribution coefficients for Sr^{2+} ($K_d = 2.3 \times 10^4$ mL g^{-1}) and Co^{2+} ($K_d = 5.6 \times 10^4$ mL g^{-1}) at pH 7. Although KCaP prefers to adsorb Co^{2+}, it can efficiently remove Sr^{2+} and Co^{2+} in the presence of multiple competing cations. Adsorption on KCaP is believed to occur as a two-stage ion-exchange process: fast exchange with K^+ and subsequent progressive exchange with Ca^{2+}. As a result of the uptake of Sr^{2+} and Co^{2+}, KCaP was transformed into chemically more stable Sr- and Co-containing CaPs. The non-reactivity of the used adsorbent makes the disposal of radioactive wastes manageable and relieves the environmental burden.

1. Introduction

The generation of large volumes of radioactive wastewater by nuclear power plants (NPP) and the 2011 accident at the Fukushima Daiichi Nuclear Power Plant (FDNPP) have drawn attention to the need for effectively remediating nuclear liquid wastes. ^{90}Sr ($t_{1/2}$ = 28.79 years) and ^{60}Co ($t_{1/2}$ = 5.27 years) are two harmful radionuclides found in cooling fluids discharged from NPPs during normal operation [1] and in water tanks at FDNPP [2]. These radionuclides are generally in their cationic form in water, allowing them to easily penetrate the food chain and accumulate in the human body. ^{90}Sr intake negatively affects the myeloid system leading to death [3] while ^{60}Co assimilation causes DNA damage through the production of reactive oxygen species [4]. Hence, these radionuclides must be removed to protect the environment and human health. Because both radioactive Sr^{2+} and Co^{2+} are present in radioactive wastewater, removing them simultaneously can simplify the treatment process. In addition, the resulting low-volume solid waste can be converted into stable ceramic waste.

Adsorption is one of the most commonly used techniques to remove radionuclides because it is cost-effective; various materials can adsorb trace pollutants from water [5]. In recent years, phosphate (PO_4^{3-})-containing materials have attracted great interest in the adsorption of radionuclides because they are suitable for further immobilization [6]. Calcium phosphates (CaPs) have been extensively investigated for Sr^{2+} removal owing to the similar chemical properties of Ca^{2+} and Sr^{2+}. For example, hydroxyapatite ($Ca_{10}(PO_4)_6(OH)_2$, HAp), the main mineral constituent of bones and teeth, can adsorb Sr^{2+} and Co^{2+} via ion exchange with Ca^{2+}. However, their adsorption capacities are low because of their compact structures [7,8]. Unlike HAp, layered dicalcium phosphate dihydrate ($CaHPO_4{\cdot}2H_2O$, DCPD) has a relatively looser crystal structure in which interlayer channels can promote the migration of ions. Consequently, DCPD exhibits higher adsorption capacities for Sr^{2+} and Co^{2+} than HAp [9,10]. However, DCPD exhibits slow uptake kinetics because its adsorption performance mostly relies on the slow release of Ca^{2+} ions from the structure.

Therefore, we hypothesized that application of a loosely layered CaP with multiple exchangeable cations could result in fast uptake kinetics and high adsorption capacities for Sr^{2+} and Co^{2+}. Layered potassium

* Corresponding authors.
E-mail addresses: aumsuh@kigam.re.kr (Y.J. Suh), kukcho@pusan.ac.kr (K. Cho).

https://doi.org/10.1016/j.seppur.2022.121789
Received 20 May 2022; Received in revised form 12 July 2022; Accepted 20 July 2022
Available online 25 July 2022
1383-5866/© 2022 Elsevier B.V. All rights reserved.

calcium phosphate ($K_3HCa(PO_4)_2$, KCaP) has a glaserite structure [11], which has a $[Ca(PO_4)_2]$ layer with an atomic arrangement different from that of the $[CaHPO_4]$ layer in DCPD. Compared with HAp (1.67) and DCPD (1.00), KCaP has a lower Ca/P ratio (0.50), resulting from the Ca vacancies occupied by K and H ions. These additional cations function as active sites for ion exchange. The use of layered KCaP with intercalated cations to adsorb Sr^{2+} and Co^{2+} is still unexplored and opens a direct route to new effective CaP-based adsorbents.

In this work, layered KCaP with multiple exchangeable ions was synthesized and used for Sr^{2+} and Co^{2+} adsorption for the first time with the expectation of enhanced adsorption performance. The effects of the contact time, initial concentration, pH, and competing cations on Sr^{2+} and Co^{2+} adsorption were explored. The structural transformations of KCaP involved in the removal of Sr^{2+} and Co^{2+} from aqueous solutions were also examined.

2. Material and methods

The reagents and characterization methods used in this study are provided in the Supporting Information (SI). Owing to safety concerns, non-radioactive stable Sr^{2+} and Co^{2+} ions served as substitutes for ^{90}Sr and ^{60}Co. All experiments were performed in triplicate, unless otherwise indicated.

2.1. Preparation of KCaP

In typical synthesis, $Ca(OH)_2$ (13.6 mmol, 1.06 g), $K_2HPO_4{\cdot}3H_2O$ (34.0 mmol, 7.84 g), KOH (6.8 mmol, 0.45 g), and 5 mL deionized water were mixed in a Teflon-lined autoclave and stirred with a magnetic stirrer for 10 min. The resulting mixture was heated to 160 °C for 24 h and then cooled to room temperature before the product was collected. The solid product was washed three times with deionized water via centrifugation to remove unreacted chemicals, vacuum-dried at 60 °C for 24 h, ground using an agate mortar and pestle, and stored in a sealed glass vial. The yield was approximately 80.2 % (3.81 g) with respect to the amount of $Ca(OH)_2$.

2.2. Batch adsorption experiments

Sr^{2+} and Co^{2+} solutions of different concentrations (C_o = 50–1000 mg L^{-1}) were prepared by dissolving appropriate amounts of $SrCl_2{\cdot}6H_2O$ and $Co(NO_3)_2{\cdot}6H_2O$, respectively, in deionized water (DIW). The pH values were adjusted using 0.5 mol L^{-1} NaOH or 0.5 mol L^{-1} HCl. A batch adsorption experiment was conducted by mixing 20 mg of KCaP powder with 20 mL of an aqueous Sr^{2+} or Co^{2+} solution in a 30 mL glass vial. The mixture was shaken using an orbital shaker (SHO-2D, Daihan Scientific Co., ltd., South Korea) at 25 °C for a certain time (t = 5–1440 min).

The effect of pH on Sr^{2+} and Co^{2+} adsorption on KCaP was explored at C_o = 100 mg L^{-1} and initial pH values of 3–11. To investigate the distribution coefficients (K_d values, mL g^{-1}) of KCaP, Sr^{2+}- and Co^{2+}-spiked aqueous Na^+, K^+, Mg^{2+}, and Ca^{2+} solutions (1.0–100 mmol L^{-1}) were used. The removal efficiency (R, %) was determined using Sr^{2+}- and Co^{2+}-spiked tap water (TWs) and artificial seawater (ASWs, Coralife®, USA). The compositions of raw TW and ASW are summarized in Table S1.

The adsorption capacity (q_e, mg g^{-1}), R, and K_d were calculated using Eqs. (1), (2), and (3) where C_o and C_e are the initial and equilibrium concentrations (mg L^{-1}), respectively, V (L) is the volume of the aqueous Sr^{2+} or Co^{2+} solution, and m (g) is the mass of the adsorbent.

$$q_e = \frac{C_o - C_e}{m} \times V \quad (1)$$

$$R = \frac{C_o - C_e}{C_o} \times 100 \quad (2)$$

$$K_d = \frac{C_o - C_e}{C_e} \times \frac{V}{m} \times 1000 \quad (3)$$

2.3. Analysis

Liquid samples were collected using 30 mL plastic syringes (SciLab Korea Co., ltd., South Korea) with 0.22 μm cellulose acetate syringe filters (Advantec, Toyo Roshi Kaisha, ltd., Japan). Portions of the filtrate were diluted into solutions containing 2.5 % w/v HNO_3 and 0.2 % w/w K^+ for Sr^{2+} or into solutions of 2.5 % w/v HNO_3 for Co^{2+}. Analyses of Sr and Co in the diluted samples were performed using flame atomic absorption spectroscopy (AAS, AAnalyst 200, PerkinElmer, Inc., USA). Elemental analyses of the samples were performed to examine the adsorption mechanisms using inductively coupled plasma optical emission spectroscopy (ICP-OES, Optima 8300, PerkinElmer, USA). Approximately 5 mL of each filtrate was used for the pH measurements (Orion Star A211 pH meter (X21407), Thermo Scientific, Indonesia).

3. Results

3.1. Properties of KCaP

The effect of the molar ratio of the $K_2HPO_4{\cdot}3H_2O$ precursor used in the synthesis of KCaP on the adsorption capacity for Sr^{2+} and Co^{2+} was examined to select an appropriate adsorbent. Samples prepared using < 5.0 mol of $K_2HPO_4{\cdot}3H_2O$ showed irregular shapes in the field emission scanning electron microscopy (FE-SEM) images (Fig. S1(a) and (b)) and lower crystallinity in their X-ray diffraction (XRD) patterns compared to the reference XRD pattern of crystalline KCaP (ICDD: 00-015-0091, Fig. S1(e)). The low crystallinity probably indicates that the particles had irregular lamellar structures with less phosphorus. On the other hand, the XRD pattern of the sample produced using 5.0 mol of $K_2HPO_4{\cdot}3H_2O$ showed characteristic Bragg peaks at 2θ = 12.12°, 24.21°, 31.24°, 31.57°, 36.56°, and 43.45°, which correspond to (001), (002), (112), (202), (003), and (–222) planes, respectively, of the reference KCaP XRD pattern (Fig. S1(e)), which is a monoclinic crystal system with a $C2/m$ space group. The addition of more $K_2HPO_4{\cdot}3H_2O$ (7.0 mol) slightly reduced the crystallinity of the sample (Fig. S1(e)), which suggests partial deterioration of the layered structure. FE-SEM images for 5.0 and 7.0 mol of $K_2HPO_4{\cdot}3H_2O$ as shown in Fig. S1(c) and (d) showed similar flake-like particles of 2.0–3.0 μm in width. Finally, the adsorption capabilities of the prepared adsorbent samples were verified by estimating their adsorption capacities. The highest adsorption capacity was observed for the sample synthesized using 5.0 mol of $K_2HPO_4{\cdot}3H_2O$ (Fig. S1(f)). Consequently, a $Ca(OH)_2$:$K_2HPO_4{\cdot}3H_2O$:KOH molar ratio of 2:5:1 was selected for preparing KCaP in subsequent experiments.

The selected KCaP samples were further characterized to identify their physicochemical properties. Energy dispersive X-ray spectroscopy (EDS) maps (Fig. 1(a)) revealed uniform distributions of the constituent elements and a K:Ca:P molar ratio of 2.94:1:2, similar to the atomic ratio in crystalline KCaP. The presence of phosphates was confirmed by the appearance of characteristic vibrational peaks at 565 cm^{-1} and 1038 cm^{-1} in the spectra of Fourier transform infrared spectroscopy (FTIR) in Fig. 1(b) [12]. The broad band ranging from 3300 to 3700 cm^{-1} pertains to the water of crystallization and the water molecules adsorbed on the KCaP.

The porosity and specific surface area of the KCaP sample were examined using N_2 adsorption–desorption isotherms (Fig. 1(c)). The isotherms were type IV Brunauer–Emmett–Teller (BET) isotherms with an H_3 hysteresis loop at PP_o^{-1} = 0.52. The BET surface area was 1.85 $m^2\ g^{-1}$ and the mean pore size was estimated to be about 15.44 nm from the Barrett–Joyner–Halenda (BJH) pore size distribution (Fig. 1(c) inset). Despite the mesoporous structure, the specific surface area was low, probably because the diffusion of N_2 molecules was blocked by the

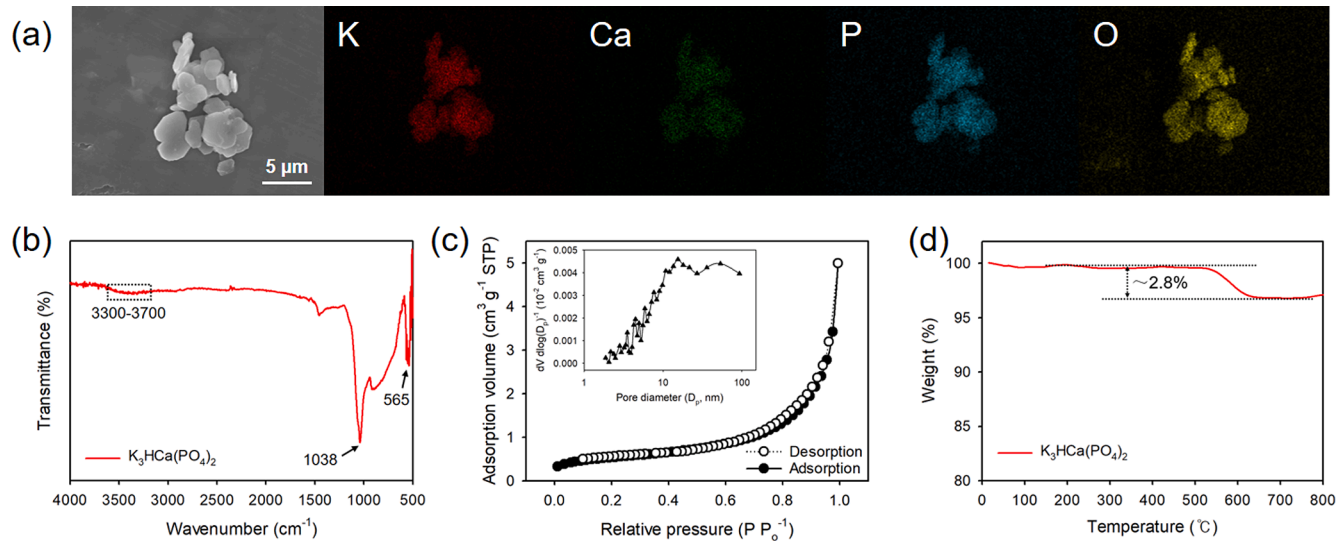

Fig. 1. Characteristics of KCaP synthesized at the optimum molar ratio of precursors: (a) FE-SEM image and EDS maps, (b) FTIR spectrum, (c) N_2 adsorption and desorption isotherms (inset: pore size distribution), and (d) thermogravimetric analysis.

K^+ and H^+ ions positioned along the KCaP channels.

Thermal stability was examined by thermogravimetric analysis of the KCaP sample (Fig. 1(d)). The as-prepared KCaP sample was stable up to $T = 560$ °C and then decomposed into pyrophosphate with an increase in temperature above 560 °C [13]. Decomposition was completed at approximately 600 °C and became stable, leaving only 2.8 % of the total weight loss.

3.2. Sr^{2+} and Co^{2+} adsorption performances of KCaP

The kinetics of Sr^{2+} and Co^{2+} uptake by KCaP were investigated by batch adsorption experiments conducted at t = 5–1440 min and C_o = 100 and 1000 mg L^{-1}. Fig. 2(a) and (b) show that Sr^{2+} and Co^{2+} adsorption on KCaP at C_o = 100 mg L^{-1} reached equilibrium within 2 h (R_{Sr} = 94.1 %) and 10 min (R_{Co} = 96.6 %), respectively. At a much higher concentration of C_o = 1000 mg L^{-1}, the adsorption of Sr^{2+} and Co^{2+} both rapidly increased in the first 4 h and plateaued after 24 h (R_{Sr}

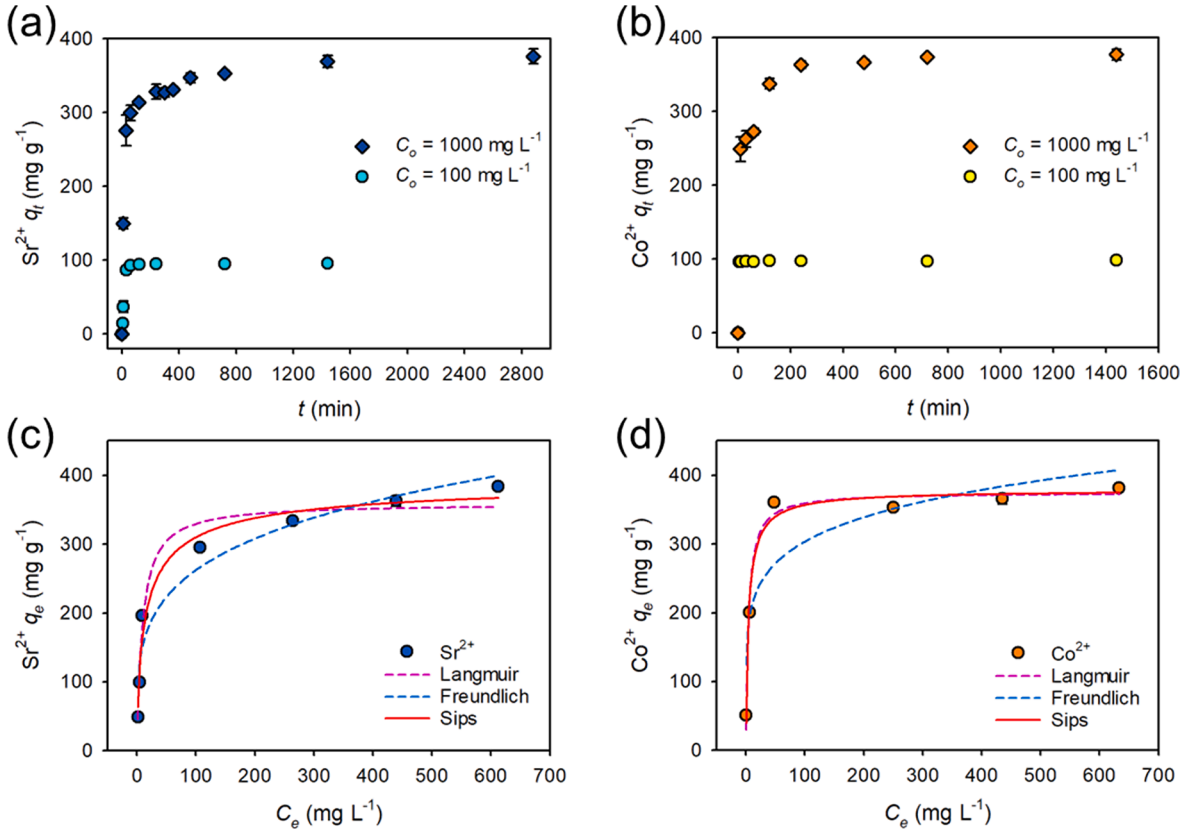

Fig. 2. Adsorption performances of KCaP toward Sr^{2+} and Co^{2+}: Effect of contact time (a) Sr^{2+} and (b) Co^{2+} (C_o = 100 and 1000 mg L^{-1}, pH = 7); Effect of initial concentration (c) Sr^{2+} and (d) Co^{2+} (pH = 7, t_{Sr} = 1440 min, t_{Co} = 480 min). General adsorption conditions: T = 25 °C, S/L = 1.0 g L^{-1}, shaking rate = 150 rpm.

= 95.6 %) and 8 h (R_{Co} = 85.0 %), respectively. The stabilized removal efficiencies were 95.57 % and 85.04 %, respectively. The reason why Co^{2+} uptake was faster than that of Sr^{2+} is discussed in Section 4.1.

Adsorption experiments at various initial concentrations of Sr^{2+} and Co^{2+} were performed to obtain the maximum adsorption capacity of KCaP. Fig. 2(c) and (d) show that the adsorption of Sr^{2+} and Co^{2+} became saturated. The adsorption capacities for Sr and Co and q_e^{Sr} and q_e^{Co}, at C_o = 1000 mg L^{-1} were 384 and 382 mg g^{-1}, respectively. The Sips model best fitted the nonlinear regressions for both the adsorption isotherms, with correlation coefficient r^2 values of 0.975 for Sr^{2+} and 0.988 for Co^{2+} (Table 1). The model fittings and their n_S values greater than 1.0 suggest that heterogeneous or multilayer adsorption of Sr^{2+} and Co^{2+} on KCaP occurred. The computed maximum Sips adsorption capacities (q_m) of KCaP for Sr^{2+} and Co^{2+} were 397 mg g^{-1} (4.53 mmol g^{-1}) and 379 mg g^{-1} (6.43 mmol g^{-1}), respectively.

The initial pH values might cause aqueous metal ions to precipitate as hydroxides, which leads to a strong bias in the removal performance. To exclude the precipitation of Sr^{2+} and Co^{2+} into metal hydroxides, experiments were conducted in the pH range of 3 to 11 for Sr^{2+} and 3 to 7 for Co^{2+}. The species distributions of Sr^{2+} and Co^{2+} as a function of pH, which were predicted by Visual MINTEQ software version 3.1 (Fig. S2) show that Sr^{2+} and Co^{2+} ions are the main species in the pH range less than 12 and 8.5, respectively. In addition, the structural integrity of the synthesized adsorbent, which affects the adsorption performance, was verified by the XRD patterns of the samples kept at pH = 3–11 (Fig. 3(a)). Adsorption experiments under varying pH conditions showed that KCaP effectively removed Sr^{2+} and Co^{2+} at those pH values (Fig. 3(b)). Notably, lower Sr^{2+} removal efficiencies were observed at pH values of 3 and 11 due to competition with either H^+ or Na^+ ions for the adsorption sites, respectively. On the other hand, the removal efficiencies for Co^{2+} were similar in the pH range of 3–7, indicating that the presence of H^+ ions under acidic conditions did not influence Co^{2+} adsorption on KCaP. For both Sr^{2+} and Co^{2+}, subsequent batch adsorption experiments were conducted at pH 7, where the highest removal efficiencies (R_{Sr} = 95.9 %, R_{Co} = 98.3 %) and K_d values (K_d^{Sr} = 2.3 × 10^4 mL g^{-1}, K_d^{Co} = 5.6 × 10^4 mL g^{-1}) were observed (Fig. 3(b)).

The adsorptive removal of Sr^{2+} and Co^{2+} from water can be inhibited by typical coexisting cations, such as Na^+, K^+, Mg^{2+}, and Ca^{2+}. With an increase in the concentration of such coexisting ions from 1.0 to 100 mmol L^{-1}, the K_d values for both Sr^{2+} and Co^{2+} decreased (Fig. 4(a) and (b)). In the presence of 100 mmol L^{-1} Na^+ ions, the K_d values for Sr^{2+} and Co^{2+} declined to 6.1 × 10^3 mL g^{-1} and 2.3 × 10^4 mL g^{-1}, respectively. On the other hand, the coexistence of 100 mmol L^{-1} K^+ ions significantly decreased the K_d^{Sr} value to 340 mL g^{-1}, which is two orders of magnitude lower, but the same amount of K^+ moderately decreased the K_d^{Co} value to 2.2 × 10^4 mL g^{-1}, which was 39 % of that in the absence of coexisting ions. The influence of divalent cations appeared to be much more significant than that of monovalent cations, the reason for which is discussed in Section 4.2. Overall, the coexisting cations inhibited Sr^{2+} and Co^{2+} adsorption on KCaP in the order $Ca^{2+} > Mg^{2+} \gg K^+/Na^+$.

Table 1
Adsorption isotherm constants for Sr^{2+} and Co^{2+} on KCaP.

Model	Parameter	Value	
		Sr^{2+}	Co^{2+}
Langmuir	q_m (mg g^{-1})	359	375
	K_L (L mg^{-1})	0.111	0.228
	r^2	0.969	0.987
Freundlich	K_F (mg g^{-1}(L $mg^{-1})^{1/n}$)	90.2	146
	n_F	4.31	6.27
	r^2	0.940	0.832
Sips	q_m (mg g^{-1})	397	379
	K_S (L $mg^{-1})^n$	0.159	0.272
	n_S	1.48	1.13
	r^2	0.975	0.988

To evaluate the potential KCaP application in real water systems, the removal efficiencies were examined for Sr^{2+}- and Co^{2+}-spiked local TW and ASW (Table S2), and the results are shown in Fig. 4(c). The R values of KCaP in DIW (a single-metal aqueous solution), TW, and ASW containing 50 mg L^{-1} Sr^{2+} were estimated to be 98.2 %, 99.6 %, and 48.8 %, respectively, and the R values in those containing 50 mg L^{-1} Co^{2+} were 99.0 %, 99.2 %, and 55.5 %, respectively. Although significant decreases in the R values for ASW were observed, KCaP outperformed previously investigated adsorbents, such as alginate/Fe_3O_4 [14] and DCPD [9]. Overall, KCaP effectively removed Sr^{2+} and Co^{2+} from contaminated water systems, even in the presence of high concentrations of competing cations.

Adsorption preferences of KCaP for Sr^{2+} and Co^{2+} were evaluated in terms of the separation factor (SF) using binary-component aqueous solutions. SF is the ratio of the K_d values of the target adsorbates [15], that is, K_d^{Co}/K_d^{Sr}. The SF values remained around 8, even at a twofold higher Sr^{2+} molar concentration (Fig. 4(d)), indicating that KCaP prefers the uptake of Co^{2+} over Sr^{2+}.

3.3. Structural transformations of KCaP

The loosely stacked structure of KCaP may be vulnerable to structural damage upon adsorption of foreign species. The structural changes in KCaP during adsorption were investigated at Sr^{2+} and Co^{2+} concentrations of C_o = 20, 100, and 1000 mg L^{-1} using elemental compositions, FE-SEM images, and EDS, FTIR, and XRD spectra. At low Sr^{2+} and Co^{2+} concentrations (C_o = 20 mg L^{-1}), the adsorbate-loaded KCaP maintained its structural integrity and morphology (Fig. 5(a)–(c)), whereas elemental analyses of the adsorption filtrates showed a greater release of K^+ ions than the adsorbed metals (Table S3). At C_o = 100 mg L^{-1}, the Sr^{2+}- and Co^{2+}-loaded adsorbents exhibited flower-like and rougher surface morphologies, respectively (Fig. 5(c)). The adsorption of Sr^{2+} and Co^{2+} resulted in a reduction in the intensities of the characteristic Bragg peaks and their complete disappearance, respectively (Fig. 5(a) and (b)). These observations suggest partial and complete structural transformations of KCaP upon exposure to 100 mg L^{-1} Sr^{2+} and Co^{2+}, respectively. At a much higher initial concentration of 1000 mg L^{-1}, KCaP was transformed into new monoclinic phases: strontium calcium phosphate ($(Sr_{0.9}Ca_{0.1})_3(PO_4)_2$, SrCaP) and cobalt phosphate octahydrate ($Co_3(PO_4)_2{\cdot}8H_2O$, CPO), as indicated by the XRD patterns (Fig. 5 (a) and (b)). These transformations were also confirmed by the SEM-EDS maps of the constituent elements (Fig. S3) and FTIR spectra (Fig. S4). According to the XRD patterns of solid residues collected after different contact times (Fig. 5(a) and (b)), KCaP was transformed into crystalline phases via amorphous phases. Upon adsorbing the Co^{2+} ions, ion exchange caused KCaP to change into an amorphous phase in just 10 min and into the crystalline phase in the subsequent 50 min. The transformation during Co adsorption occurred much faster than that during Sr adsorption, which is congruent with the fast kinetics of Co^{2+} adsorption. Consequently, recrystallization was completed in 24 h and 8 h on the adsorption of Sr^{2+} and Co^{2+}, respectively.

4. Discussion

4.1. Effects of layer structure and exchangeable cations

A loosely-layered structure of KCaP may facilitate the effusion of interlayered and structural cations, resulting in faster uptake kinetics than DCPD, even though the standard interlayer spacing of KCaP (7.43 Å) is similar to that of DCPD (7.59 Å). KCaP with a glaserite structure consists of $[Ca(PO_4)_2]$ layers in which the three O atoms of the PO_4 tetrahedron are shared with the adjacent CaO_6 octahedron, and the remaining O atom does not participate in bridge bonding (Fig. 6(a)). This configuration accounts for the negative charge of the $[Ca(PO_4)_2]$ layer, forming a more loosely stacked structure with charge-

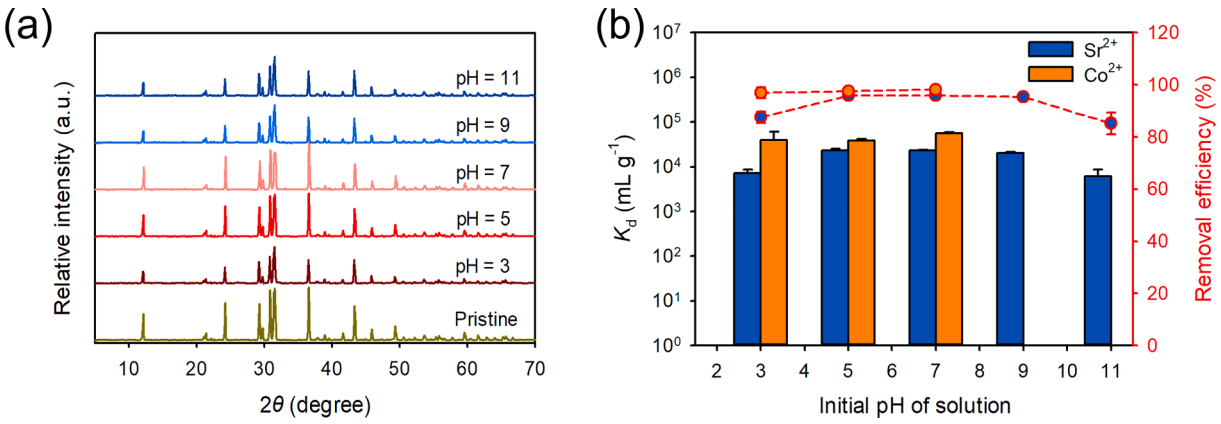

Fig. 3. Influence of pH on the adsorption performances of KCaP toward Sr^{2+} and Co^{2+}: (a) XRD patterns and (b) distribution coefficients and removal efficiencies (C_o = 100 mg L^{-1}, t_{Sr} = 1440 min, t_{Co} = 480 min). General adsorption conditions: T = 25 °C, S/L = 1.0 g L^{-1}, shaking rate = 150 rpm.

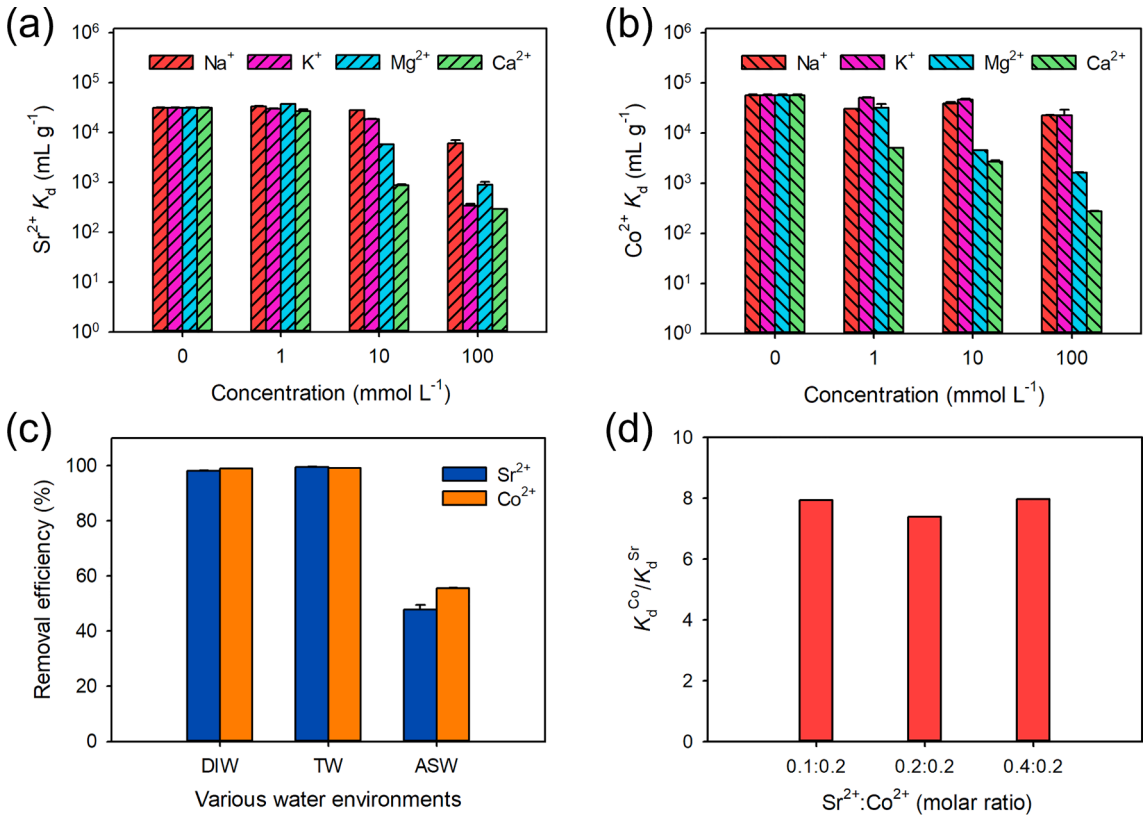

Fig. 4. Sr^{2+} and Co^{2+} uptake performance of KCaP: Influence of increasing concentrations of coexisting ions on (a) Sr^{2+} and (b) Co^{2+} adsorption ($C_o \cong$ 100 mg L^{-1}, t_{Sr} = 1440 min, t_{Co} = 480 min); (c) Sr^{2+} and Co^{2+} removal efficiencies in various model aqueous solutions ($C_o \cong$ 50 mg L^{-1}, t_{Sr} = 1440 min, t_{Co} = 480 min); and (d) separation factors (K_d^{Co}/K_d^{Sr}) in binary-component aqueous solutions (C_o^{Sr} = 0.1–0.4 mmol L^{-1}, C_o^{Co} = 0.2 mmol L^{-1}, t = 1440 min). General adsorption conditions: pH = 7, T = 25 °C, and S/L = 1.0 g L^{-1}.

compensating cations of K^+ and H^+ (Fig. 6(b)), which is different from the [$CaHPO_4$] layers of DCPD (Fig. S5(a) and (c)). The interlayered cations have coordination numbers of either 12 or 10, indicated as K(1) and K(2) sites in Fig. 6(b), respectively. Fig. S5(e) and (f) provide detailed views of these K sites.

As noted in Section 3.2, the adsorption of Co^{2+} on KCaP at C_o = 100 mg L^{-1} reached equilibrium in 10 min, which was much faster than 24 h for that on DCPD at a lower initial concentration of C_o = 50 mg L^{-1} [9]. A higher initial Co^{2+} concentration may cause a longer equilibration time for KCaP because an increase in the Co^{2+} concentration from 100 to 1000 mg L^{-1} prolonged the equilibration time from 10 min to 8 h in this study. Meanwhile, the adsorption of Sr^{2+} on KCaP at C_o = 100 mg L^{-1} reached equilibrium in 2 h, which was much slower than that of Co^{2+} on KCaP. The observed equilibration time for Sr^{2+} was, however, much shorter than that for Co^{2+} adsorption on DCPD. Therefore, KCaP provides much faster adsorption kinetics for both Co^{2+} and Sr^{2+} than DCPD because of its structural advantages.

In addition to the structural Ca^{2+} ions, the presence of exchangeable interlayer K^+ ions provided KCaP with greater adsorption capacities than DCPD and HAp, whose adsorption performances mostly rely on their structural Ca^{2+} ions. The adsorption capacity of KCaP for Co^{2+} (382 mg g^{-1}) was remarkably higher than that of DCPD (285 mg g^{-1}) at

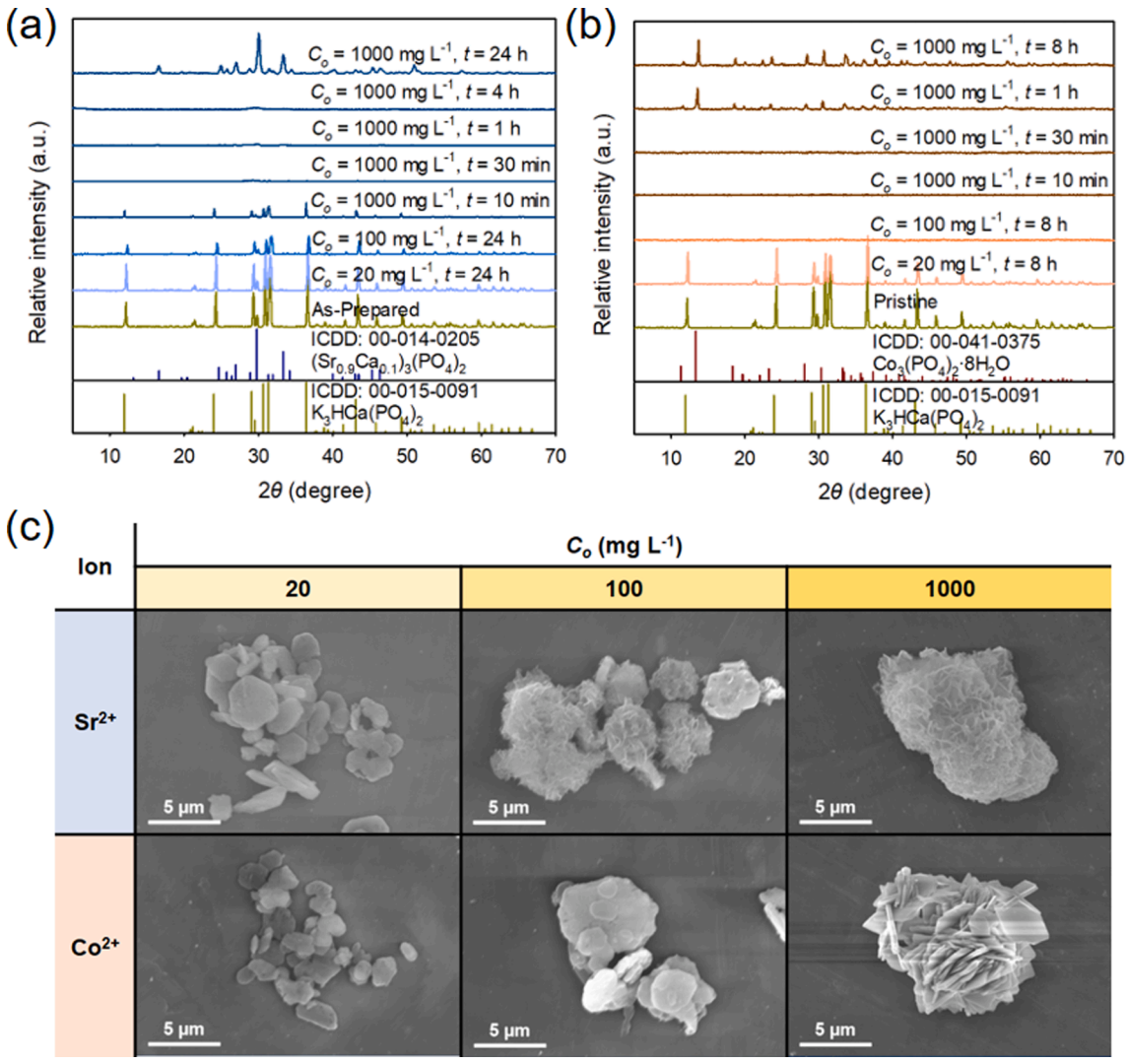

Fig. 5. Changes in the structural property and surface morphology of KCaP: XRD patterns of (a) Sr^{2+}- and (b) Co^{2+}-loaded adsorbents at different t and C_o values; (c) FE-SEM images of the adsorbents collected after adsorption at C_o = 20–1000 mg L^{-1}.

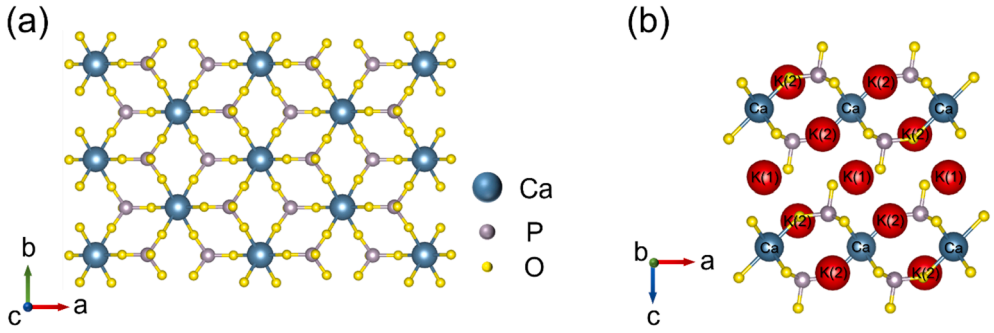

Fig. 6. Illustration of $K_3HCa(PO_4)_2$ structure: views of the (a) $[Ca(PO_4)_2]$ layer along the c-axis and (b) stacked layers with interlayer cations, K(1) and K(2), along the b-axis. Illustrations were generated using VESTA ver. 3.5.5 [16] with CIF taken from Grenier et al. [17].

C_o = 1000 mg L^{-1} [9]. Compared with other adsorbents (Fig. 7), the highest q_e value of KCaP for Sr^{2+} (384 mg g^{-1}) was higher than that of previously reported adsorbents, such as A-ZrP (320 mg g^{-1}) [18], flower-like-α-ZrP (291 mg g^{-1}) [19], Na-A-1000 kGy (237 mg g^{-1}) [20], Ca-Mg phosphate (218 mg g^{-1}) [21], titanate nanowires (175 mg g^{-1}) [22], KTS-3 (105 mg g^{-1}) [23], FJSM-InMOF (39 mg g^{-1}) [24], and NaZTS (44 mg g^{-1}) [25], but lower than that of GO-HAp (551 mg g^{-1}) [26]. In addition, the highest q_e value of KCaP for Co^{2+} (382 mg g^{-1}) was also higher than that of ozonized graphene oxide (322 mg g^{-1}) [27], DCPD (285 mg g^{-1}) [9], (MB-IA)-g-MNCC (187 mg g^{-1}) [28], and the composite CpAD adsorbent (185 mg g^{-1}) [29] but lower than that of PoP600 (405 mg g^{-1}) [30], as shown in Fig. 7. Regarding the simultaneous removal of Sr^{2+} and Co^{2+}, the adsorption capacities of KCaP were much higher than those of previously studied adsorbents (Fig. 7), such as

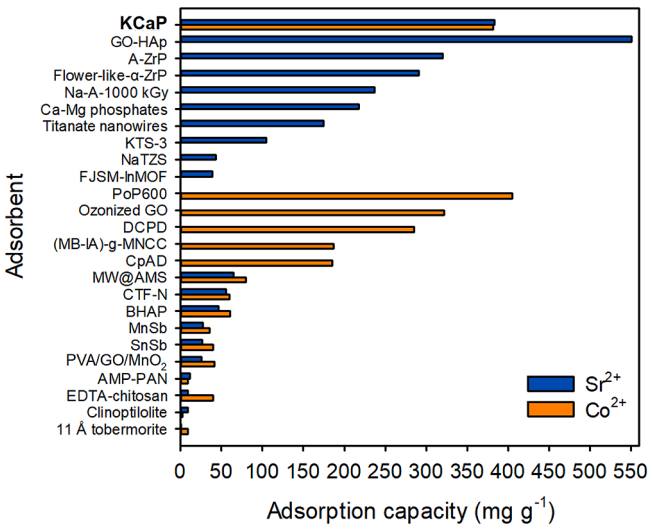

Fig. 7. Comparison of the highest q_e values of different Sr^{2+} and Co^{2+} adsorbents. The highest q_e values were estimated from the pertinent figures of the references through the WebPlotDigitizer ver. 4.5.

MW@AMS [31], covalent triazine framework [32], BHAp [33], SnSb [34], MnSb [35], AMP-PAN [36], EDTA-chitosan [37], clinoptilolite [38], 11 Å tobermorite [39], and PVA/GO/MnO_2 [40].

The K_d values of KCaP are compared to those of previously investigated adsorbents (Table S3). The K_d toward Sr^{2+} of KCaP is higher than that of Fe_3O_4/GO [41], GO-HAp [26], and HAp [8], but lower than that of A-ZrP [18]. On the other hand, the K_d toward Co^{2+} of KCaP is higher than that of Slag-Ox [42], DCPD, and PoP600 [30], but lower than that of NaAlg-HAp-CNT [43].

4.2. Adsorption mechanism

The mechanism of Sr^{2+} and Co^{2+} adsorption on KCaP was explored using FE-SEM, EDS, XRD, FTIR, and ICP-OES for the adsorbents and adsorptive solutions before and after the adsorption experiments. EDS maps revealed that adsorption at C_o = 1000 mg L^{-1} resulted in a dramatic decline in K and Ca contents and homogeneous spread of Sr and Co on the surface of the adsorbents (Fig. S3). The Sr-loaded adsorbent exhibited an additional FTIR spectral peak at 854 cm^{-1} (Fig. S4(a)), which was ascribed to the P—O—P asymmetric stretching of SrCaP [9]. On the other hand, the FTIR spectrum of the Co-loaded adsorbent showed characteristic peaks at 1032, 974, and 937 cm^{-1}, which were ascribed to the PO_4 bond found in CPO (Fig. S4(b)) [44]. In addition, the XRD patterns of SrCaP (Fig. 5(a), ICDD: 00–014-0205) and CPO (Fig. 5(b), ICDD: 00–041-0375) are also shown. Upon adsorption at a low initial concentration of C_o = 20 mg L^{-1}, only K^+ ions were exchanged with Sr^{2+} or Co^{2+} ions; however, at higher concentrations, both K^+ and Ca^{2+} participated in the ion exchange (Table S3). Therefore, the adsorption of Sr^{2+} and Co^{2+} on KCaP primarily occurs through ion exchange with interlayer K^+ and structural Ca^{2+}, resulting in structural transformations of KCaP at high adsorptive concentrations. Moreover, we hypothesize that the adsorption of divalent cations (M^{2+}) on KCaP via ion exchange results in bidentate complexation with ≡PO^- groups (Eq. (4)), which is similar to the adsorption mechanism of DCPD [9,10].

$$2(\equiv PO^-)_{(s)} + M^{2+}_{(aq)} + nH_2O \rightarrow (\equiv PO^-)_2M{\cdot}nH_2O_{(s)} \quad (4)$$

Electrostatic interactions and chemical hardness (η) are believed to be the key driving forces in the enhanced Sr^{2+} and Co^{2+} adsorption on KCaP. Co^{2+} has a smaller ionic radius (r_i = 0.65 Å) than K^+ (r_i = 1.38 Å) and Ca^{2+} (r_i = 1.00 Å) whereas Sr^{2+} has an intermediate ionic radius (r_i = 1.18 Å). Therefore, divalent Co^{2+} ions have greater Coulombic interactions with O on the KCaP surface than both K^+ and Ca^{2+}, whereas Sr^{2+} has an intermediate degree of interaction. The complexation of Sr^{2+} and Co^{2+} on the interlayer of KCaP can be further elucidated by introducing the hard and soft acids and bases theory or the concept of chemical hardness [45,46]. The O near K^+ of KCaP has higher electron density than its parent O element (η = 6.08 eV), because of the low electronegativity of K^+ (0.82 in Pauling scale), making it a weaker hard Lewis base where local hardness was used for bases [47]. Hence, this weakly hard O prefers weakly hard Lewis acids to borderline Lewis acids, such as Sr^{2+} (η = 16.30 eV) and Co^{2+} (η = 8.21 eV). The η values were calculated using a previously reported equation by Parr and Pearson [48]. Even under acidic conditions (pH = 3), Co^{2+} did not show a decrease in the distribution coefficient, as monovalent H^+ is a harder acid. Thus, these two concepts explain why Co^{2+} has a higher distribution coefficient than Sr^{2+} during ion exchange with K^+ (η = 13.64 eV) and Ca^{2+} (η = 19.52 eV) on KCaP.

These two driving forces can also explain the inhibitory effect of coexisting ions on Sr^{2+} and Co^{2+} adsorption (Fig. 4(a)–(c)). The monovalent cations, Na^+ (η = 21.08 eV) and K^+, probably have less chemical association with the O of KCaP because of their charge; hence, relatively less influence of Na^+ on the Sr^{2+} K_d value (6.1 × 10^3 mL g^{-1}) was observed even at a high concentration (100 mmol L^{-1}). However, at a high K^+ concentration (100 mmol L^{-1}), the Sr^{2+} K_d value significantly decreased to 340 mL g^{-1} likely because of the pronounced restrictive interference of K^+ as K^+ has an η value closer to that of Sr^{2+} than Na^+. In contrast, Co^{2+} is a borderline acid favored by the weakly hard O of KCaP. This explains why Co^{2+} adsorption did not decline in the presence of monovalent cations even at high concentrations (K_d^{Co} = 2.2 × 10^4–2.3 × 10^4 mL g^{-1}). The influence of electrostatic interactions appears to be much stronger in the presence of divalent competing ions. At Mg^{2+} and Ca^{2+} concentrations of 100 mmol L^{-1}, significant decreases in K_d values down to 290–884 mL g^{-1} for Sr^{2+} and 272–1.59 × 10^3 mL g^{-1} for Co^{2+} were observed. A higher ionic concentration corresponds to a higher ionic strength, which leads to thinning of the electrical double layer and thus reduces electrostatic interactions. The ionic strength of a solution is given by the summation of the product of the concentration and square of the charge of the ions. Likewise, the adsorption in ASW resulted in considerable decreases in the K_d values to K_d^{Sr} = 954 mL g^{-1} and K_d^{Co} = 1.25 × 10^3 mL g^{-1} (Fig. 4(c)). Among divalent cations, Ca^{2+} interferes with the adsorption of Sr^{2+} and Co^{2+} more strongly than Mg^{2+} (η = 32.55 eV) because of its relatively low hardness. The lower chemical hardness of Co^{2+} compared to Sr^{2+} is also the primary cause for its preferential removal by KCaP from the binary component (Sr^{2+}/Co^{2+}) solutions (Fig. 4(d)). Therefore, the phosphate of KCaP may have a higher chemical affinity for Co^{2+} than Sr^{2+} and the other cations considered in this study.

Notably, the replacement of interlayer K^+ and structural Ca^{2+} ions with Sr^{2+} and Co^{2+} at $C_o \geq$ 100 mg L^{-1} led to the structural transformation of KCaP. The faster transformation of KCaP upon exposure to Co^{2+} ions in water can be explained in terms of the ionic radius and chemical hardness. Co^{2+} has smaller ionic radius (r_i = 0.65 Å) and lower hardness (η = 8.21 eV) than Sr^{2+} (r_i = 1.18 Å, η = 16.30 eV), allowing it to diffuse faster through the KCaP channels and be preferentially associated with the weakly-hard O of KCaP [49]. The release of the interlayer K^+ ions and subsequent adsorption of the target divalent cations could have led to either partial collapse or complete decomposition of KCaP. A similar behavior was also observed in a previous study on DCPD [50]. As illustrated in Fig. 8, Co^{2+} adsorption on KCaP was henceforth used as a model for a simpler explanation of the structural transformation. At C_o = 1000 mg L^{-1}, the early 10 min-long Co^{2+} uptake transformed KCaP into amorphous cobalt phosphate (ACP), which subsequently crystallized into CPO at 1 h, as revealed by the change in the XRD patterns with time (Fig. 5(b)). This transformation was accompanied by the release of K^+ and Ca^{2+} from the structure of KCaP (Table S2). The progressive exchange between Ca^{2+} and Co^{2+} is supposed to occur to shorten the distance between the cation and the oxygen at the PO_4 tetrahedron,

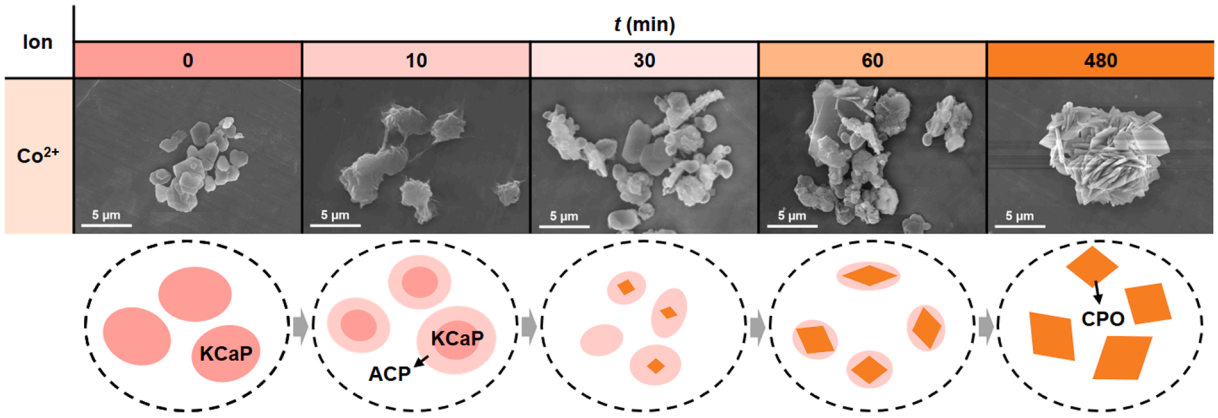

Fig. 8. FE-SEM images of transient structural transformations of KCaP and a schematic diagram of the phase transitions during Co^{2+} adsorption (C_o = 1000 mg L^{-1}, t = 0–480 min).

resulting in the formation of new bonds between phosphate and Co^{2+} ions, thereby converting the short-range-order phase of ACP into the long-range order phase of the new crystal, CPO [51]. Because of its metastability, ACP can spontaneously crystallize into HAp in aqueous solutions [52,53]. However, the presence of Co^{2+} ions in the aqueous solution led to a more stable phase of CPO than HAp. The structural transformation during Sr^{2+} adsorption may proceed at a slower rate via the same route as that of Co^{2+} adsorption.

Considering the practical applications of radioactive Sr^{2+} and Co^{2+} removal, the final radioactive products of SrCaP and CPO should be treated carefully. Fortunately, calcium phosphate ($Ca_3(PO_4)_2$) and cobalt phosphate ($Co_3(PO_4)_2$) are sparingly soluble in water, as indicated by their solubility products of about 2.07 × 10^{-33} and 2.05 × 10^{-35}, respectively [55]. In addition, the capability of KCaP to effectively adsorb both Sr^{2+} and Co^{2+} reduces the production volume of solid waste that retains the radionuclides. Additionally, CaP can be easily converted into ceramics for disposal in geological repositories. These advantages suggest the potential application of KCaP for the treatment of radioactive materials.

5. Conclusions

In this study, we hypothesized that layered KCaP with a loose structure and multiple exchangeable cations would have rapid uptake kinetics and high capacities for the adsorption of Sr^{2+} and Co^{2+}. As expected, KCaP exhibited rapid uptakes of 94.1 % Sr^{2+} and 96.6 % Co^{2+} in 120 min and 10 min, respectively, and high adsorption capacities of 384 mg g^{-1} for Sr^{2+} and 382 mg g^{-1} for Co^{2+}. Although KCaP strongly prefers the uptake of Co^{2+}, it can efficiently remove both Sr^{2+} and Co^{2+} from water containing various competing cations. The mechanism of its high distribution coefficient for Sr^{2+} and Co^{2+} over competing cations is well explained in terms of electrostatic interaction and chemical affinity between the adsorbent and adsorbates. Notably, a large amount of adsorbates resulted in the transformation of KCaP into more chemically stable SrCaP and CPO. In conclusion, KCaP has a high potential for sequestering multiple radionuclides from water, enabling improved radioactive waste management.

Funding

This work was supported by the Basic Science Research Program through the National Research Foundation funded by the Ministry of Education, Republic of Korea [2020R1A6A1A03044834; 2022R1I1A3063150] and the Basic Research Project [GP2020-013, 22–3212] of the Korea Institute of Geoscience and Mineral Resources (KIGAM) funded by the Ministry of Science and ICT of Korea.

CRediT authorship contribution statement

Zeqiu Li: Methodology, Formal analysis, Writing – original draft. **Eleazer L. Vivas:** Writing – review & editing. **Chenyang Yang:** Writing – review & editing. **Yong Jae Suh:** Validation, Investigation, Writing – review & editing. **Kuk Cho:** Conceptualization, Supervision, Funding acquisition.

Declaration of Competing Interest

The authors declare that they have no known competing financial interests or personal relationships that could have appeared to influence the work reported in this paper.

Data availability

Data will be made available on request.

Appendix A. Supplementary material

Supplementary data to this article can be found online at https://doi.org/10.1016/j.seppur.2022.121789.

References

[1] A. Panov, A. Trapeznikov, V. Trapeznikova, A. Korzhavin, Influence of operation of thermal and fast reactors of the Beloyarsk NPP on the radioecological situation in the cooling pond. Part 1: Surface water and bottom sediments, Nuclear Eng. Technol. (2022).
[2] J. Vives i Batlle, The potential impact of marine discharges from Fukushima 10 years after the accident, Integrated Environmental Assessment and Management (2022).
[3] R.D. Ray, D.M. Thomson, N.K. Wolff, D. LaViolette, BONE METABOLISM II. Toxicity and metabolism of radioactive strontium (Sr^{90}) in Rats, JBJS 38 (1) (1956) 160–174.
[4] N. Gault, C. Sandre, J.L. Poncy, C. Moulin, J.L. Lefaix, C. Bresson, Cobalt toxicity: Chemical and radiological combined effects on HaCaT keratinocyte cell line, Toxicol. In Vitro 24 (1) (2010) 92–98, https://doi.org/10.1016/j.tiv.2009.08.027.
[5] R. Chakraborty, A. Asthana, A.K. Singh, B. Jain, A.B.H. Susan, Adsorption of heavy metal ions by various low-cost adsorbents: a review, Int. J. Environ. Anal. Chem. (2020) 1–38.
[6] M.G. Mesko, D.E. Day, B.C. Bunker, Immobilization of CsCl and SrF_2 in iron phosphate glass, Waste Manage. 20 (4) (2000) 271–278, https://doi.org/10.1016/S0956-053X(99)00331-1.
[7] I. Smiciklas, I. Dimovic, M. Mitric, Removal of Co^{2+} from aqueous solutions by hydroxyapatite, Water Res. 40 (12) (2006) 2267–2274, https://doi.org/10.1016/j.watres.2006.04.031.
[8] J. Kim, N.S. Sambudi, K. Cho, Removal of Sr^{2+} using high-surface-area hydroxyapatite synthesized by non-additive in-situ precipitation, J. Environ. Manage. 231 (2019) 788–794, https://doi.org/10.1016/j.jenvman.2018.10.100.
[9] E.L. Vivas, K. Cho, Efficient adsorptive removal of Cobalt(II) ions from water by dicalcium phosphate dihydrate, J. Environ. Manage. 283 (2021) 111990, https://doi.org/10.1016/j.jenvman.2021.111990.

[10] E.L. Vivas, L. Sumin, C. Kuk, Brushite-infused polyacrylonitrile nanofiber adsorbent for strontium removal from water, J. Environ. Manage. 270 (2020) 110837, https://doi.org/10.1016/j.jenvman.2020.110837.

[11] R. Nikolova, V. Kostov-Kytin, Crystal chemistry of "glaserite" type compounds, Bul. Chem. Commun. 45 (2013) 418–426.

[12] A. Massit, A. El Yacoubi, A. Kholtei, B.C. El Idrissi, XRD and FTIR analysis of magnesium substituted tricalcium calcium phosphate using a wet precipitation method, Biointerface Res. Appl. Chem. 11 (2021) 8034–8042.

[13] A. Dyer, D. Leigh, F.T. Ocon, Studies on crystalline zirconium phosphate-I: ion-exchanged forms of α-zirconium phosphate, J. Inorg. Nucl. Chem. 33 (1971) 3141–3151.

[14] H.J. Hong, H.S. Jeong, B.G. Kim, J. Hong, I.S. Park, T. Ryu, K.S. Chung, H. Kim, J. Ryu, Highly stable and magnetically separable alginate/Fe_3O_4 composite for the removal of strontium (Sr) from seawater, Chemosphere 165 (2016) 231–238, https://doi.org/10.1016/j.chemosphere.2016.09.034.

[15] J.L. Mertz, Z.H. Fard, C.D. Malliakas, M.J. Manos, M.G. Kanatzidis, Selective Removal of Cs^+, Sr^{2+}, and Ni^{2+} by $K_{2x}MgxSn_{3-x}S_6$ (x = 0.5–1) (KMS-2) Relevant to Nuclear Waste Remediation, Chemistry of Materials 25 (10) (2013) 2116–2127. https://doi.org/10.1021/cm400699r.

[16] K. Momma, F. Izumi, VESTA: a three-dimensional visualization system for electronic and structural analysis, J. Appl. Crystallogr. 41 (3) (2008) 653–658, https://doi.org/10.1107/S0021889808012016.

[17] J.-C. Grenier, A. Durif-Varambon, C. Martin, Structure cristalline de $CaK_3H(PO_4)_2$, Bull. Minér. (1969) 30–32.

[18] Z. Li, E.L. Vivas, Y.J. Suh, K. Cho, Highly efficient and selective removal of Sr^{2+} from aqueous solutions using ammoniated zirconium phosphate, J. Environ. Chem. Eng. 10 (2) (2022) 107333.

[19] W. Mu, Q. Yu, R. Zhang, X. Li, R. Hu, Y. He, H. Wei, Y. Jian, Y. Yang, Controlled fabrication of flower-like α-zirconium phosphate for the efficient removal of radioactive strontium from acidic nuclear wastewater, J. Mater. Chem. A 5 (46) (2017) 24388–24395, https://doi.org/10.1039/c7ta07803j.

[20] J. Chen, M. Zhang, J. Shu, M. Yuan, W. Yan, P. Bai, L. He, N. Shen, S. Gong, D. Zhang, Electron beam irradiation-induced formation of defect-rich zeolites under ambient condition within minutes, Angew. Chem. Int. Ed. 60 (27) (2021) 14858–14863.

[21] I.L. Shashkova, A.I. Ivanets, N.V. Kitikova, M. Sillanpää, Effect of phase composition on sorption behavior of Ca-Mg phosphates towards Sr(II) ions in aqueous solution, J. Taiwan Inst. Chem. Eng. 80 (2017) 787–796, https://doi.org/10.1016/j.jtice.2017.09.027.

[22] Y. Ishikawa, S. Tsukimoto, K.S. Nakayama, N. Asao, Ultrafine sodium titanate nanowires with extraordinary Sr ion-exchange properties, Nano Lett. 15 (5) (2015) 2980–2984, https://doi.org/10.1021/nl504820c.

[23] D. Sarma, C.D. Malliakas, K.S. Subrahmanyam, S.M. Islam, M.G. Kanatzidis, $K_{2x}Sn_{4-x}S_{8-x}$(x=0.65-1): a new metal sulfide for rapid and selective removal of Cs^+, Sr^{2+} and UO_2^{2+} ions, Chemical Science 7(2) (2016) 1121-1132. https://doi.org/10.1039/c5sc03040d.

[24] Y.-J. Gao, M.-L. Feng, B. Zhang, Z.-F. Wu, Y. Song, X.-Y. Huang, An easily synthesized microporous framework material for the selective capture of radioactive Cs^+ and Sr^{2+} ions, J. Mater. Chem. A 6 (9) (2018) 3967–3976, https://doi.org/10.1039/c7ta11208d.

[25] M. Zhang, P. Gu, S. Yan, L. Dong, G. Zhang, Na/Zn/Sn/S (NaZTS): Quaternary metal sulfide nanosheets for efficient adsorption of radioactive strontium ions, Chem. Eng. J. 379 (2020) 122227, https://doi.org/10.1016/j.cej.2019.122227.

[26] T. Wen, X. Wu, M. Liu, Z. Xing, X. Wang, A.-W. Xu, Efficient capture of strontium from aqueous solutions using graphene oxide–hydroxyapatite nanocomposites, Dalton Trans. 43 (20) (2014) 7464–7472.

[27] X. Liu, Y. Huang, S. Duan, Y. Wang, J. Li, Y. Chen, T. Hayat, X. Wang, Graphene oxides with different oxidation degrees for Co(II) ion pollution management, Chem. Eng. J. 302 (2016) 763–772, https://doi.org/10.1016/j.cej.2016.05.107.

[28] T.S. Anirudhan, F. Shainy, J.R. Deepa, Effective removal of Cobalt(II) ions from aqueous solutions and nuclear industry wastewater using sulfhydryl and carboxyl functionalised magnetite nanocellulose composite: batch adsorption studies, Chem. Ecol. 35 (3) (2018) 235–255, https://doi.org/10.1080/02757540.2018.1532999.

[29] M.R. Awual, M.M. Hasan, A. Islam, A.M. Asiri, M.M. Rahman, Optimization of an innovative composited material for effective monitoring and removal of cobalt(II) from wastewater, J. Mol. Liq. 298 (2020) 112035, https://doi.org/10.1016/j.molliq.2019.112035.

[30] G.Z. Kyzas, E.A. Deliyanni, K.A. Matis, Activated carbons produced by pyrolysis of waste potato peels: cobalt ions removal by adsorption, Colloids Surf., A 490 (2016) 74–83.

[31] H. Fakhri, A.R. Mahjoub, H. Aghayan, Effective adsorption of Co^{2+} and Sr^{2+} ions by 10-tungsten-2-molybdophosphoric acid supported amine modified magnetic SBA-15, J. Radioanal. Nucl. Chem. 321 (2) (2019) 449–461, https://doi.org/10.1007/s10967-019-06595-6.

[32] Y. Yu, L. Zhou, J. Tang, P. Wu, L. Feng, B. Ge, H. Chen, J. Hu, S. Song, T. Zeng, Effective removal of Co(II) and Sr(II) from radiocative wastes using covalent triazine frameworks: Kinetics and isotherm studies, Sep. Purif. Technol. 277 (2021) 119633, https://doi.org/10.1016/j.seppur.2021.119633.

[33] S. Handley-Sidhu, T.K. Mullan, Q. Grail, M. Albadarneh, T. Ohnuki, L.E. Macaskie, Influence of pH, competing ions and salinity on the sorption of strontium and cobalt onto biogenic hydroxyapatite, Sci. Rep. 6 (1) (2016) 23361, https://doi.org/10.1038/srep23361.

[34] L. Zhang, J. Wei, X. Zhao, F. Li, F. Jiang, M. Zhang, X. Cheng, Competitive adsorption of strontium and cobalt onto tin antimonate, Chem. Eng. J. 285 (2016) 679–689, https://doi.org/10.1016/j.cej.2015.10.013.

[35] L. Zhang, J. Wei, X. Zhao, F. Li, F. Jiang, M. Zhang, X. Cheng, Removal of strontium (II) and cobalt(II) from acidic solution by manganese antimonate, Chem. Eng. J. 302 (2016) 733–743, https://doi.org/10.1016/j.cej.2016.05.040.

[36] Y. Park, Y.-C. Lee, W.S. Shin, S.-J. Choi, Removal of cobalt, strontium and cesium from radioactive laundry wastewater by ammonium molybdophosphate–polyacrylonitrile (AMP–PAN), Chem. Eng. J. 162 (2) (2010) 685–695, https://doi.org/10.1016/j.cej.2010.06.026.

[37] S. Zhuang, Q. Zhang, J. Wang, Adsorption of Co^{2+} and Sr^{2+} from aqueous solution by chitosan grafted with EDTA, J. Mol. Liq. 325 (2021) 115197, https://doi.org/10.1016/j.molliq.2020.115197.

[38] I. Smičiklas, S. Dimović, I. Plećaš, Removal of Cs^{1+}, Sr^{2+} and Co^{2+} from aqueous solutions by adsorption on natural clinoptilolite, Appl. Clay Sci. 35 (1) (2007) 139–144, https://doi.org/10.1016/j.clay.2006.08.004.

[39] N.J. Coleman, D.S. Brassington, A. Raza, A.P. Mendham, Sorption of Co^{2+} and Sr^{2+} by waste-derived 11 Å tobermorite, Waste Manage. 26 (3) (2006) 260–267, https://doi.org/10.1016/j.wasman.2005.01.019.

[40] J. Huo, G. Yu, J. Wang, Efficient removal of Co(II) and Sr(II) from aqueous solution using polyvinyl alcohol/graphene oxide/MnO_2 composite as a novel adsorbent, J. Hazard. Mater. 411 (2021) 125117, https://doi.org/10.1016/j.jhazmat.2021.125117.

[41] X. Wang, J. Yu, Application of Fe_3O_4/graphene oxide composite for the separation of Cs (I) and Sr (II) from aqueous solution, J. Radioanal. Nucl. Chem. 303 (1) (2015) 807–813.

[42] Q.T.N. Le, E.L. Vivas, K. Cho, Oxalated blast-furnace slag for the removal of Cobalt (II) ions from aqueous solutions, J. Ind. Eng. Chem. 95 (2021) 57–65.

[43] F. Karkeh-Abadi, S. Saber-Samandari, S. Saber-Samandari, The impact of functionalized CNT in the network of sodium alginate-based nanocomposite beads on the removal of Co (II) ions from aqueous solutions, J. Hazard. Mater. 312 (2016) 224–233.

[44] H.Y. Li, H.W. Yu, J.L. Zhai, L. Sun, H.J. Yang, S.H. Xie, Self-assembled 3D cobalt phosphate octahydrate architecture for supercapacitor electrodes, Mater. Lett. 152 (2015) 25–28, https://doi.org/10.1016/j.matlet.2015.03.053.

[45] Y.J. Suh, J.W. Chae, H.D. Jang, K. Cho, Role of chemical hardness in the adsorption of hexavalent chromium species onto metal oxide nanoparticles, Chem. Eng. J. 273 (2015) 401–405, https://doi.org/10.1016/j.cej.2015.03.095.

[46] R.G. Pearson, Hard and soft acids and bases, J. Am. Chem. Soc. 85 (22) (1963) 3533–3539, https://doi.org/10.1021/ja00905a001.

[47] R.G. Pearson, Absolute electronegativity and hardness: application to inorganic chemistry, Inorg. Chem. 27 (4) (1988) 734–740, https://doi.org/10.1021/ic00277a030.

[48] R.G. Parr, R.G. Pearson, Absolute hardness: companion parameter to absolute electronegativity, J. Am. Chem. Soc. 105 (26) (1983) 7512–7516, https://doi.org/10.1021/ja00364a005.

[49] Y. Sugiura, Y. Saito, T. Endo, Y. Makita, Effect of the ionic radius of alkali metal ions on octacalcium phosphate formation via different substitution modes, Cryst. Growth Des. 19 (7) (2019) 4162–4171, https://doi.org/10.1021/acs.cgd.9b00656.

[50] E. Boanini, F. Silingardi, M. Gazzano, A. Bigi, Synthesis and hydrolysis of brushite (DCPD): the role of ionic substitution, Cryst. Growth Des. 21 (3) (2021) 1689–1697.

[51] L.W. Du, S. Bian, B.D. Gou, Y. Jiang, J. Huang, Y.X. Gao, Y.D. Zhao, W. Wen, T. L. Zhang, K. Wang, Structure of clusters and formation of amorphous calcium phosphate and hydroxyapatite: from the perspective of coordination chemistry, Cryst. Growth Des. 13 (7) (2013) 3103–3109.

[52] H. Fleisch, R.G.G. Russell, S. Bisaz, Influence of Pyrophosphate on the Transformation of amorphous to crystalline calcium phosphate, Calcif. Tissue Res. 2 (1) (1968) 49–59.

[53] H. Pan, X.Y. Liu, R. Tang, H.Y. Xu, Mystery of the transformation from amorphous calcium phosphate to hydroxyapatite, Chem. Commun. 46 (39) (2010) 7415–7417, https://doi.org/10.1039/c0cc00971g.

[54] J. Rumble, CRC Handbook of Chemistry and Physics, 99th ed., CRC Press, Boca Raton, 2018.